remote sensing

MDPI

Technical Note

Estimating Visible Band Albedo from Aerial Orthophotographs in Urban Areas

Jaroslav Hofierka * and Katarína Onačillová

Institute of Geography, Faculty of Science, Pavol Jozef Šafárik University in Košice, 041 54 Košice, Slovakia; katarina.onacillova@upjs.sk

* Correspondence: jaroslav.hofierka@upjs.sk

Abstract: Albedo is an important parameter in many environmental and renewable energy models. Satellite sensors can be used to derive broadband or narrowband albedos. However, the spatial resolution of such data can be insufficient in urban areas with complex morphology and land cover diversity. In this study, we propose the use of widely available aerial orthophotographs to derive visible band albedo in urban surfaces that can be effectively used in high-resolution applications. The solution is based on the estimation of the reflected irradiance captured by an RGB sensor and approximated by the brightness component in the hue-saturation-brightness (HSB) color model and incident solar irradiance modelled by the r.sun module in GRASS GIS. The visible band albedo values are calibrated by published reference values for selected land cover classes or, alternatively, by a spectroradiometer. The method is applied to the central part of Košice and compared to visible band albedo derived from the Landsat 8 OLI and Sentinel 2A sensors and previously published typical albedo values for various land cover classes, resulting in reasonable agreement. The proposed methodology is implemented using standard GIS tools that are easily applicable to any high-resolution urban data.

Keywords: albedo; solar radiation; orthophotographs; urban areas; Košice city

Citation: Hofierka, J.; Onačillová, K. Estimating Visible Band Albedo from Aerial Orthophotographs in Urban Areas. *Remote Sens.* **2022**, *14*, 164. https://doi.org/10.3390/rs14010164

Academic Editor: Janet Nichol

Received: 28 October 2021
Accepted: 29 December 2021
Published: 31 December 2021

1. Introduction

The importance of albedo for determination of energy balance of land surfaces is well known. Albedo determines the amount of solar radiation absorbed by the insolated material thus directly influencing land surface temperature (LST) especially in urban areas [1]. Moreover, the reflected component of solar radiation directly influenced by albedo may be significant, particularly in areas with complex surface geometry and high reflectivity (e.g., high mountains, urban areas).

The surface albedo is generally defined as the ratio of reflected sunlight to the incident sunlight received by a surface. It depends on physical properties of the surface material as well as spectral and angular distribution of the incident sunlight. Thus, the atmospheric conditions and solar rays angle affects the reflectance of light at a particular time. The broadband albedo refers to the entire spectrum of solar radiation, the spectral albedo uses a specific wavelength such as visible light (0.4–0.7 μm) or near-infrared (0.7–1.3 μm). The spectral distribution of incoming solar radiation is modified by absorption in the atmospheric liquid and vaporous water. Absorption occurs predominantly in the near-infrared (NIR) which favors visible (VIS) over NIR radiation at the surface under cloudy skies [2]. The vegetation and bare soil have higher NIR albedo than VIS albedo. In many environmental applications, the visible and near-infrared (IR) albedos are quite often needed. Sometimes these are further divided into direct and diffuse albedos [3,4].

Despite a plethora of sensors and techniques, the surface albedo is still a poorly predicted variable in many climate models and solar applications. The broadband albedo is usually estimated from low-resolution broadband sensors from the top of atmosphere

such as Nimbus-7 Earth Radiation Budget (ERB) [5], Earth Radiation Budget Experiment (ERBE) [6] and the Scanner for the Earth Radiation Budget (ScaRaB) [7]. These measurements require the knowledge of the atmospheric conditions and surface characteristics which can be monitored effectively only by multispectral sensors. The derivation of surface broadband albedos from narrowband observations from satellite platforms such as LANDSAT, Sentinel or MODIS requires several levels of processing. Important steps include atmospheric correction, angular models that convert directional reflectance to spectral albedo, and narrowband to broadband conversion [8]. However, the spatial resolution of these data can be insufficient in urban areas with complex land cover and morphology.

Determination of albedo for various land cover classes is not an easy task. Many algorithms for estimation of surface broadband albedo from satellite data have been developed [8–11]. These algorithms depend on observation technology (e.g., single-angular vs. multi-angular observation platforms or geostationary vs. polar-orbit satellites). The derived albedo data can be used for many large-scale studies such as urban heat island (UHI) effects comparing built-up vs. rural areas; however, the spatial and temporal resolution of such data can be insufficient for very detailed intra-urban applications. With the advance of high-resolution 3D city models, there is a demand for very detailed datasets covering specific urban features such as buildings and roads. Moreover, the complex urban environment contains many land cover classes as well as shadows cast by buildings and trees which make the estimation very approximate.

The aerial orthophotographs in the visible waveband of electromagnetic spectrum are commonly used in geospatial applications due to their wide availability, high spatial resolution, rich content and geometrical accuracy. They are frequently used for detailed land cover mapping for many decades [12]. They provide high-resolution image representation of a territory with corrected geometric distortions arising from the perspective projection of aerial photographs. Many countries perform a periodic mapping of their territories including orthophotographs creating vast geospatial databases stored in geographic information systems (GIS) and online map systems such as Google Earth Engine. With the advance of unmanned aerial systems (UAS), the aerial orthophotographs are increasingly available also for small area projects [13]. The orthophotographs are typically created in a visible waveband of electromagnetic spectrum (red-green-blue, RGB) with spatial resolution ranging from a few cm to tens of cm. It is this extremely high spatial resolution and geometric accuracy that makes orthophotographs attractive for mapping urban areas.

The growing interest in environmental and sustainable energy problems specifically related to urban areas such as UHI phenomenon or solar energy applications stimulates the development of simulation models requiring high-resolution geospatial data including albedo [14,15]. Albedo is an important input parameter in solar radiation and land surface temperature (LST) models. Nevertheless, the availability of high-resolution albedo data for urban areas is very rare. To address this problem, we have developed a methodology for estimation of visible band (VIS) albedo from aerial RGB orthophotographs. We present a methodology that is based on estimation of solar irradiance incident to a digital surface model (DSM) representing urban surfaces at the time of acquiring of orthophotographs as well as a conversion of the RGB images to the HSB color model to estimate the reflected radiance. The methodology is applied to the sample urban area in Košice, Slovakia and results compared to the satellite-derived data and published reference VIS albedo values of land cover classes present in the area.

2. Methods and Data

2.1. The Study Area and Data

The study area covers 4 km^2 in the central part of the Košice City in Eastern Slovakia (48°43′35″N, 21°15′20″E), with a typical Central European urban setting for city centers with diverse land cover classes including buildings with various roofs, asphalt roads and urban greenery (Figure 1). In the historic city center, the buildings have usually 3–4 floors

with occasional taller buildings such as cathedrals or theater. The study area also contains residential zones with single family detached houses, blocks of flats (5–12 floors) and commercial buildings. The typical width of streets (urban canyons) is in the range of 10–20 m. The area was mapped during several surveying campaigns in 2016 and 2017 including photogrammetric, airborne and terrestrial laser scanning data [16]. In this study, we used RGB orthophotographs and a raster-based DSM representing terrain, buildings and urban greenery derived from airborne laser scanning and photogrammetry, both at 0.5-m spatial resolution. The orthophotographs were taken on 9 August 2016, at 10:44 GMT (12:08 local solar time) using the Vexcel UltraCamXp camera with the following spectral bands: R 580–700 nm, G 480–630 nm, B 410–570 nm. The solar altitude was 57.15° and solar azimuth 183.54° measured from North clockwise. The vector-based land cover map was derived from the orthophotomosaic consisting of 23 land cover classes typical for this urban area [15]. The dominating land cover classes were roofs (27.84% of the total area), asphalt roads (25.67%), grass (20.44%) and trees (16.86%).

The spaceborne multispectral imagery of the Landsat 8 OLI sensor from 30 June 2016 09:20:19 GMT was used to derive VIS albedo using the adapted methodology proposed by Liang [8] for Landsat TM sensors (Figure 2). The calculation was completed in GRASS GIS [17,18]. The spatial resolution of VIS Landsat 8 albedo (L8 albedo) is 30 m. The Sentinel 2A sensor was used to derive VIS albedo according the methodology proposed by Li et al. [19]. Sentinel 2A Level 1C (L1C) product (tile 34UEU, 29 June 2016, acquisition time 9:40:32 GMT) was downloaded via Copernicus Open Access Hub (https://scihub.copernicus.eu/dhus/, accessed on 21 December 2021). The original L1C data representing the top-of-atmosphere spectral reflectances projected in a cartographic system (WGS84/UTM zone 34N) were processed using the Sen2Cor processor (version 2.5.5) developed by ESA to generate bottom of atmosphere reflectances, i.e., surface reflectances (termed as the Sentinel 2A Level 2A (L2A) product) at 10 m resolution for three targeted visible bands (blue—Band 2, green—Band 3, red—Band 4). To derive the VIS albedo at 10 m resolution from Sentinel 2A's three narrowband albedos, we used snow-free narrow-to-broadband (NTB) conversion coefficients published by Li et al. [19] (Figure 3).

2.2. VIS Albedo Derived from Aerial RGB Orthophotographs

In general, the broadband albedo α is defined as a ratio of reflected (I_{refl}) and incident (I_{inc}) solar irradiance [W/m^2]:

$$\alpha = I_{refl} / I_{inc} \quad (1)$$

The amount of light reflected by a surface element depends on reflectance properties of the material as well as the direction of incident solar rays and light emitted in the direction of the sensor [20]. Thus, the albedo value depends on position of the sun and sensor as well as land surface morphology. If we assume that our urban surfaces are Lambertian (isotropic in reflectance from different solar/view angles), we can calculate albedo values knowing the position of the sun and the sensor. Sensu stricto, the term 'albedo' is correct here only if the surface is Lambertian, otherwise the term 'reflectance' is more appropriate [9].

The Lambertian assumption may be far from the actual situations, especially for vegetation and glossy surfaces, however, this assumption might be acceptable for high-resolution data representing homogeneous anthropogenic urban surfaces and an approximate estimation of albedo values when multiangle observations are not available. Though not all urban surfaces are Lambertian, this is often a good approximation when the characteristics of the surfaces are unknown or for validation purposes [11].

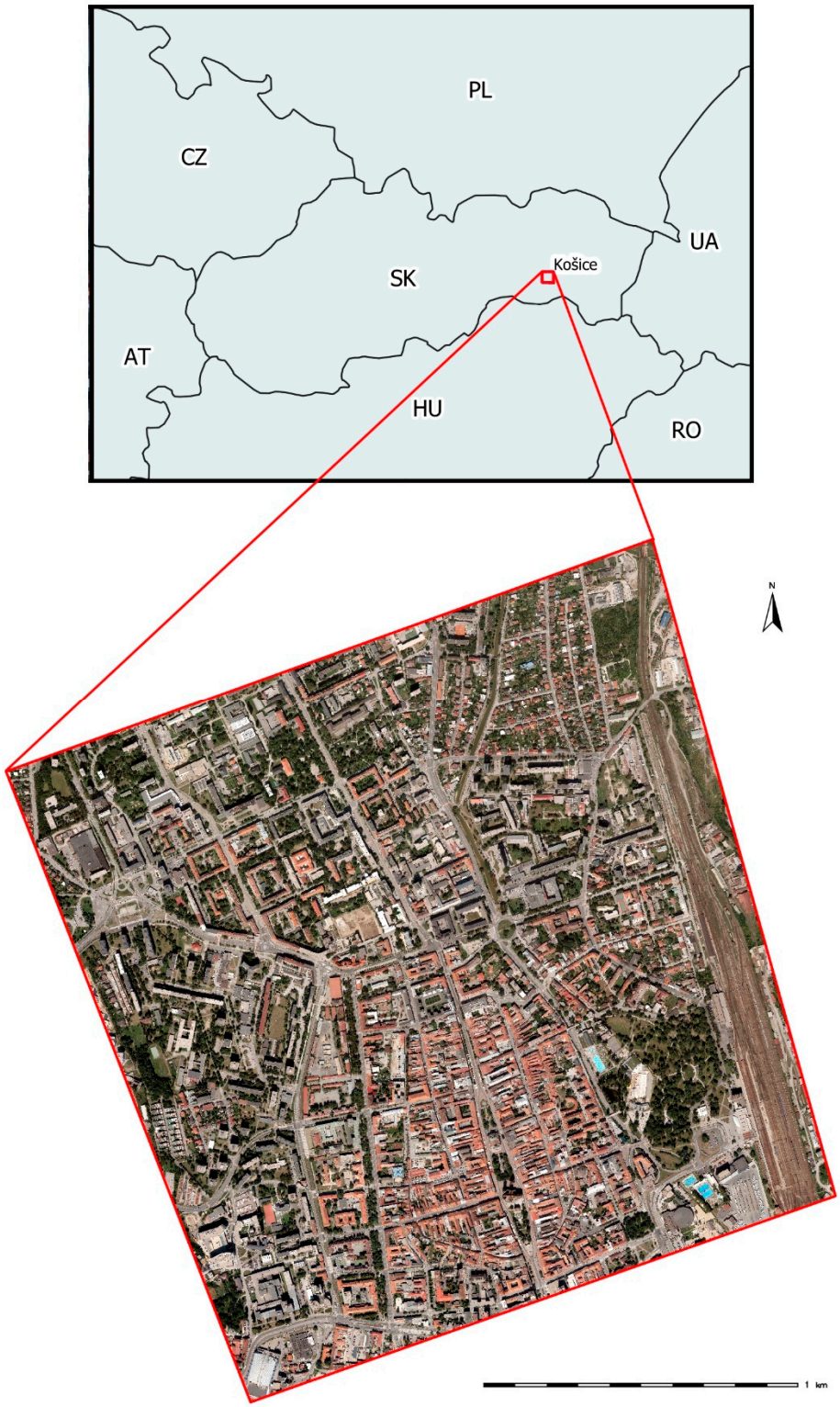

Figure 1. Location of the study area and orthophotomosaic used in this study.

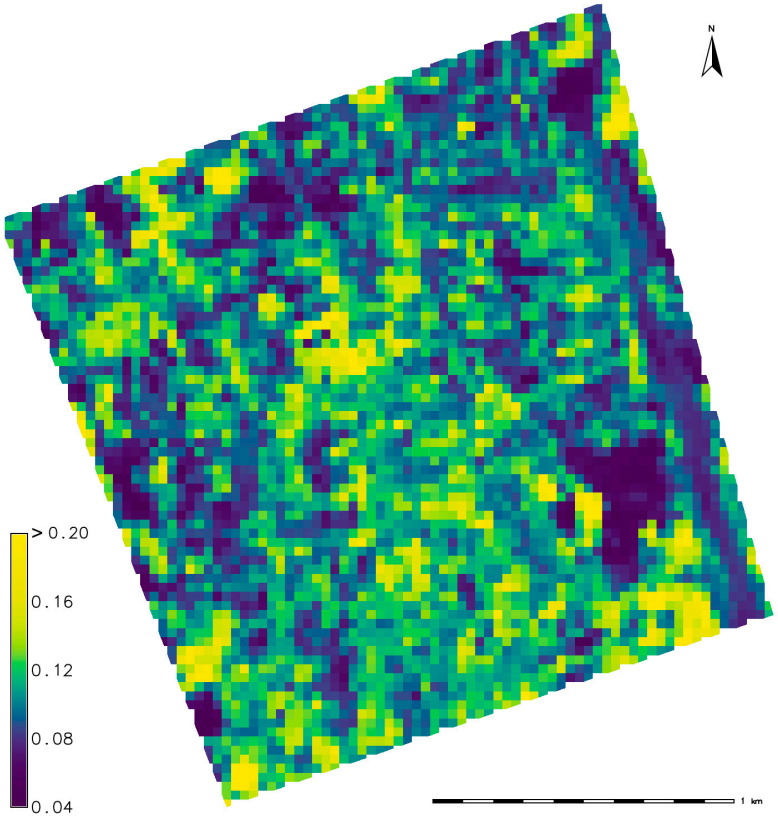

Figure 2. VIS albedo derived from the Landsat 8 OLI imagery.

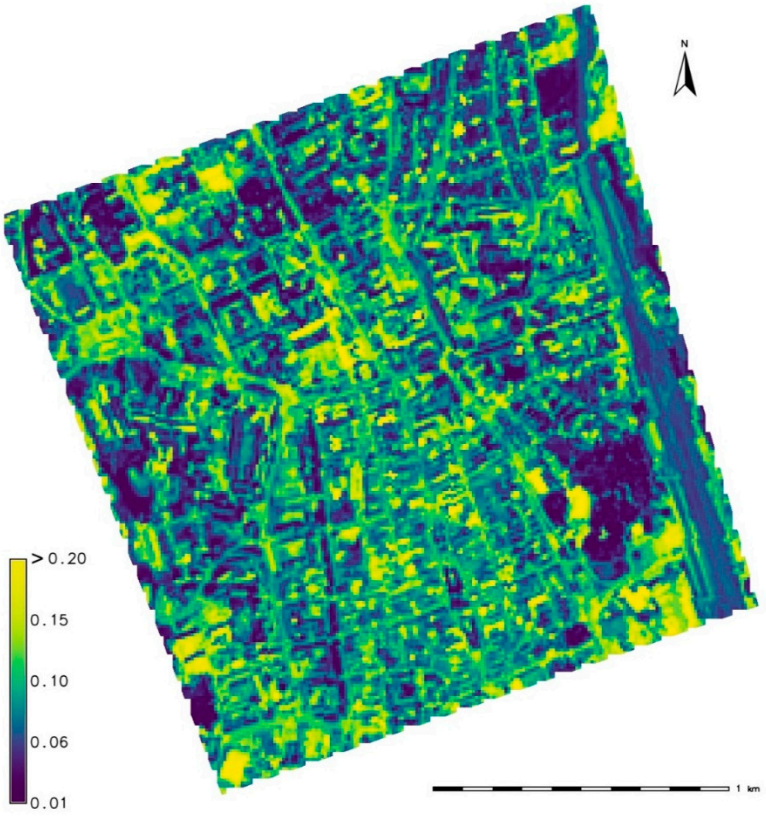

Figure 3. VIS albedo derived from the Sentinel 2A imagery.

The reflected radiance $R_{refl}(\theta)$ [W/sr/m^2] from a Lambertian surface in the direction of sensor (v) is proportional to the cosine of the emission angle θ between the sensor (v) and the surface normal (n) according to Lambert's cosine law (Figure 4):

$$R_{refl}(\theta) = R_n \cos\theta \quad (2)$$

where R_n is the radiance emitted from a surface in the direction of the surface normal (n) [W/sr/m^2]. In case of orthophotographs, we assume that the sensor is in a orthogonal position (v), i.e., $\theta = 0$ for horizontal surfaces. For inclined surfaces, θ is equal to the slope angle (γ) derived from a DSM.

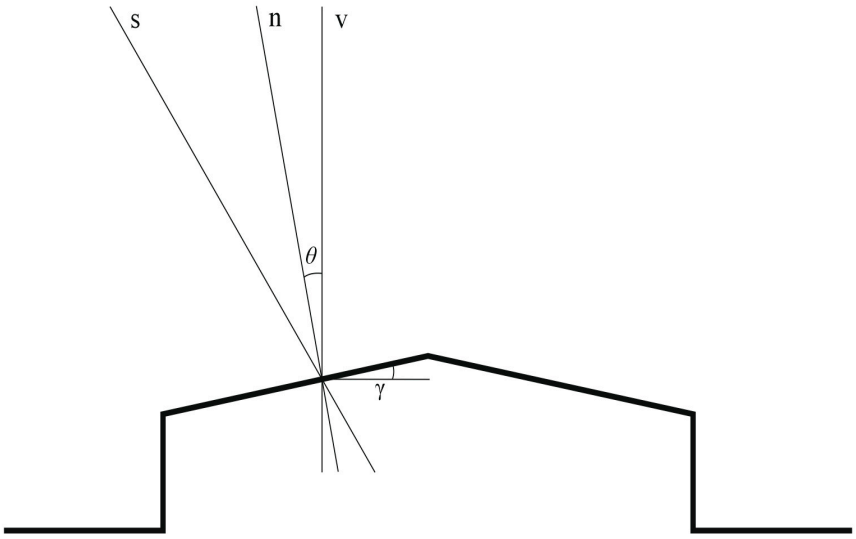

Figure 4. Orientation of incident sunlight (**s**), surface normal (**n**) and sensor (**v**). DSM is drawn by bold line.

The VIS albedo requires an estimation of reflected and incident solar irradiance in a visible waveband of electromagnetic spectrum. In our approach, the amount of incident solar irradiance is estimated using the r.sun solar radiation module in GRASS GIS [18,21]. Using this module, we can compute the total solar irradiance in three components (beam, diffuse and reflected) on inclined surfaces for any moment of time. The computed solar irradiance includes the broadband solar electromagnetic spectrum. The visible band accounts for approximately 46% of the total energy available in the solar spectrum [22] so the VIS solar irradiance incident at the time when the RGB orthophotographs were taken can be directly estimated.

The reflected irradiance I_{refl} can be estimated from the RGB orthophotographs using a standard conversion of RGB to a hue-saturation-brightness (HSB) color model and Lambert's cosine law for emitted radiance from a Lambertian surface (Equation (2)). The brightness component is defined as a visual perception how much light the surface emits [23]. The apparent brightness (radiance) of a Lambertian surface to an observer (sensor) is the same regardless of the observer's angle of view. It has the same radiance although the emitted power from a surface element is reduced by the cosine of the emission angle due to a foreshortened surface element visible to the viewer. To calculate the reflected irradiance (radiant flux per unit surface area) in the direction of sensor, the apparent brightness must be multiplied by $\cos\theta$, in our case cosine of the slope angle derived from a DSM.

Brightness is usually calculated as an arithmetic mean of the RGB color components. This can be easily calculated as a simple map algebra operation in GRASS GIS when RGB components are stored as rasters in a GIS database [18]. However, the brightness parameter provides an estimation of the reflected light in relative, not absolute terms. The reflected irradiance values derived from brightness can be calibrated to field measurements of the

VIS reflected irradiance by spectroradiometer in dominating and preferably homogeneous land cover classes or derived from the known VIS albedo values for the selected land cover classes, such as roofs, roads, grass, etc. It is not necessary to know or measure every land cover class, usually 3–4 dominating classes should be sufficient to determine the calibrating multiplication coefficient for the reflected VIS irradiance or albedo. In our case we use the latter, more convenient and straightforward approach. Our dominating reference land cover classes were asphalt roads, roofs, grass and trees (Table 1).

Table 1. Calibration coefficients for selected reference land cover classes.

Land Cover	Share of Total Area %	Uncalibrated VIS Albedo	Reference Albedo [1]	Calibration Coefficient
asphalt roads	25.67	0.195	0.098	0.502
roofs	27.84	0.163	0.098	0.601
grass	20.44	0.150	0.080	0.532
trees	16.86	0.086	0.043	0.502

[1] Published by Brest [24].

The uncalibrated VIS albedo values for each land cover class in Table 1 were calculated as spatially averaged values by zonal statistics in GRASS GIS. The reference VIS albedo values were taken from Brest [24] with similar geographical conditions indicating the calibration coefficient for each land cover class. It is interesting to note that these fraction coefficients are almost identical (asphalt roads 0.502, trees 0.502, grass 0.532, roofs 0.601). The area weighted average of calibration coefficients presented in Table 1 is 0.54 and this value is used to multiply uncalibrated, relative values of calculated VIS albedo for the whole area.

The calculated albedo for roofs can be affected by various roof shapes and materials. When a higher number of in situ measurements is available, the calibration procedure can be completed using a more sophisticated approach such as a least-squares linear regression. In the case of in situ measurements of the reflected VIS irradiance, this calibration must be completed within the brightness to irradiance conversion.

To summarize, the calculation of VIS albedo is completed in GRASS GIS using the following steps:

1. Calculation of the slope angle and slope aspect for DSM using the r.slope.aspect module;
2. Calculation of the solar irradiance incident on DSM for 9 August 12:08 local solar time using the r.sun module;
3. Calculation of brightness for the HSB color model using the r.mapcalc module;
4. Correction of brightness for inclined surfaces using the cosine of the slope angle of DSM leading to uncalibrated reflected irradiance using the r.mapcalc module;
5. Calculation of the ratio of the slope corrected brightness component and incident solar irradiance for uncalibrated VIS albedo using the r.mapcalc module;
6. Calibration of the VIS albedo according to the reference VIS albedo values for selected land cover classes using the r.mapcalc module.

The workflow is schematically shown in the flowchart (Figure 5). In case of available measured values of reflected irradiance by spectroradiometer, the slope corrected brightness parameter can be calibrated to measured reflected irradiance values for selected land cover classes and VIS albedo is computed as a ratio of calibrated slope corrected brightness and incident irradiance.

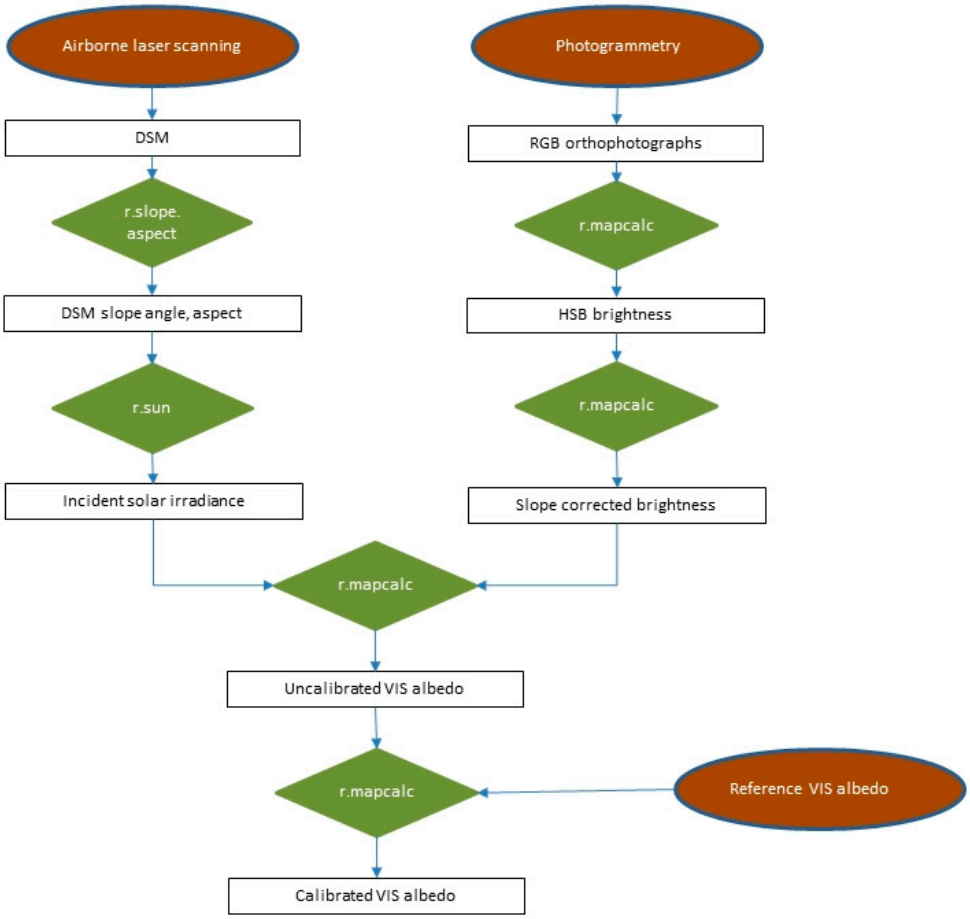

Figure 5. The flowchart of procedural steps.

3. Results

The methodology described above was applied to the data representing the inner city of Košice. The DSM and orthophotographs were prepared during our previous studies [14–16]. All calculation steps were completed in GRASS GIS. The incident solar irradiance was calculated using the r.sun solar radiation module for clear-sky conditions, with Linke's coefficient of atmospheric turbidity = 5, which is a typical value for the city with heavy industry zones present in Košice [25]. We used the reference VIS albedo values published by Brest [24] for four land cover classes dominating our study area (Table 1). The calculated VIS albedo values were calibrated using a multiplication coefficient 0.54 as shown above.

The final VIS albedo map is presented in Figure 6. The mean of VIS albedo in the study area is 0.08 with range of 0–0.73 and standard deviation 0.056. Most VIS albedo values are within the range of 0.05–0.12. The means of VIS albedo values derived from RGB orthophotographs (RGB albedo), Landsat 8 OLI (L8 albedo) and Sentinel 2A (S2 albedo) within the selected land cover classes that cover almost 91% of the total area are presented in Table 2. The RGB albedo values are the most variable in the trees (variation coefficient = 83.45%) and grass (variation coefficient = 74.58%) land cover classes. Trees is a land cover class consisting of various broad-leaved as well as coniferous trees with very complex morphology only approximately represented by a DSM.

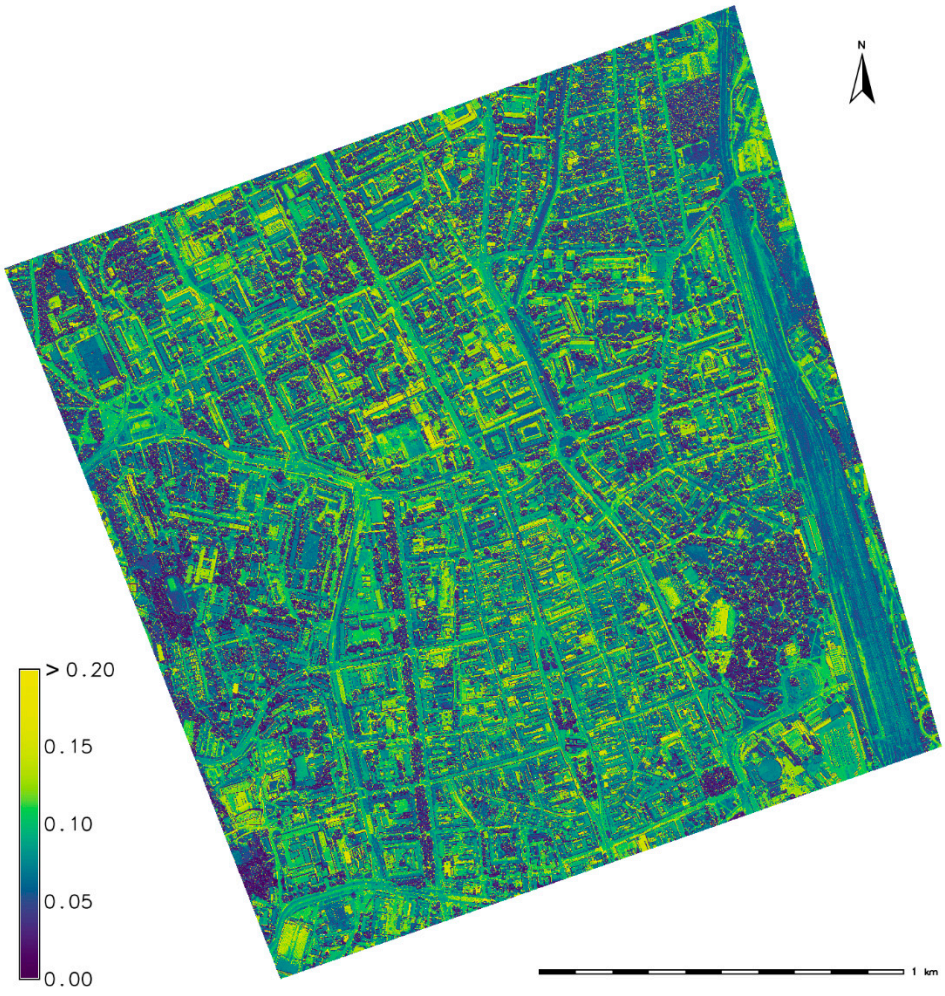

Figure 6. VIS albedo derived from the RGB orthophotographs.

Table 2. Mean VIS albedo values derived from RGB orthophotographs, Landsat 8 OLI, Sentinel 2A and published values for selected land cover classes.

Land Cover	RGB Albedo	L8 Albedo [1]	S2 Albedo [2]	Reference Albedo [3]
asphalt roads	0.106	0.116	0.112	0.098
roofs	0.088	0.115	0.103	0.098
grass	0.081	0.100	0.080	0.080
trees	0.046	0.090	0.055	0.043

[1] Derived according to Liang [8], [2] Derived according to Li et al. [19], [3] Published by Brest [24].

The zonal statistics in GRASS GIS was used to calculate mean albedo values for each reference land cover class (Table 2). The means of L8 albedo values are slightly higher, especially for trees and grass. This can be explained by very low resolution of Landsat 8 OLI data (30 m), so the pixel values usually contain also other land cover classes with higher albedo. In comparison, the means of S2 albedo for trees and grass are very close to the derived RGB albedo and reference VIS albedo values.

As we wanted to compare the calculated RGB to L8 and S2 albedos also spatially, we resampled (aggregated) the derived RGB albedo data at 0.5 m spatial resolution to 30 m and 10 m spatial resolutions of Landsat 8 OLI and Sentinel 2A, respectively. The bivariate scatterplot of cells from L8 and resampled RGB albedo rasters is presented in Figure 7. The figure indicates that VIS albedo derived from Landsat 8 OLI sensor includes some raster cells with higher values in comparison to derived VIS RGB albedo. This is associated

mostly with a few larger roofs that reflect to Landsat 8 OLI sensor more radiance at the specific Sun position when the Landsat 8 image was taken (09:20:19 GMT, 30 June 2016). The lower values of derived VIS RGB albedo for these areas can be attributed to smoothing effects of resampling technique. The Pearson's correlation coefficient is 0.7176 and root mean square error (RMSE) is 0.034 which we consider acceptable due to a different time of sensing and very large difference in spatial resolution of both rasters. The bivariate scatterplot of cells from S2 and resampled VIS RGB albedo rasters is presented in Figure 8. The S2 albedo shows a few pixels with some high albedo values mostly associated with roofs inclined to a south-east direction. This leads to a slightly lower Pearson's correlation coefficient of 0.6553 and slightly worse root mean square error (RMSE) of 0.038, which we still consider acceptable.

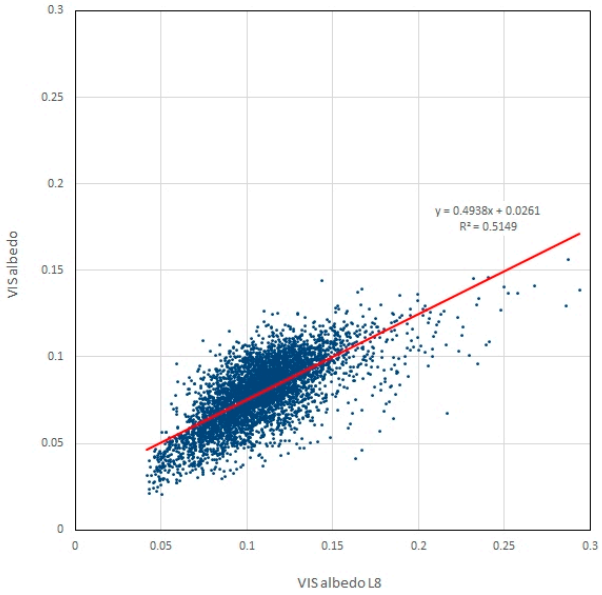

Figure 7. Scatterplot of VIS albedo derived from the RGB orthophotographs and Landsat 8 OLI imagery.

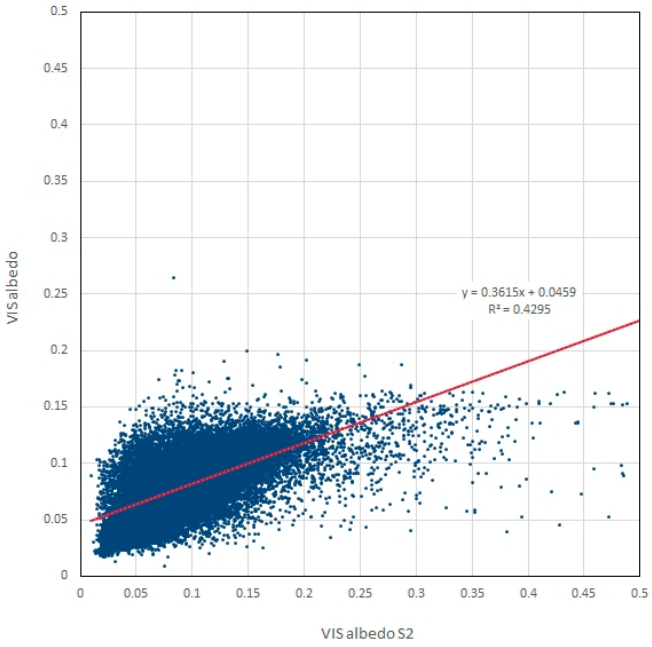

Figure 8. Scatterplot of VIS albedo derived from the RGB orthophotographs and Sentinel 2A imagery.

In contrast to a low-resolution albedo derived from satellite sensors, the presented methodology accounts also for shadows cast by tall objects such as buildings. These can be identified in Figure 9A as almost black areas adjacent to buildings from the north. Using the r.sun solar radiation model and a high-resolution DSM, the diffuse component of solar irradiance can be calculated and used in the albedo calculation according to Equation (1). The diffuse component of solar radiation usually presents 20–25% of the total solar irradiance under clear-sky conditions [26]. The brightness of the RGB image for these areas is also low, so the albedo can be calculated, though the accuracy of estimation is lower due to various factors such as unknown share of diffuse component in solar radiation at the given moment or a lower accuracy of DSM in areas with strong elevation changes (buildings, trees) (Figure 9B). The S2 albedo (Figure 9C), albeit with a higher resolution, still shows a spatial averaging on features such as buildings (outlined with a black line) or urban greenery. Perhaps the most problematic is the situation with shadowed areas adjacent to the tall buildings from the north which clearly show low albedo values (dark blue color). Most urban features are completely spatially averaged in L8 albedo (Figure 9D). This can be problematic for highly detailed intra-urban studies. For example, one of the frequent mitigation measures to lower the overheating phenomenon in cities is increasing albedo of particular roofs and streets. The analysis of such urban features is probably beyond the capability of the satellite technology used in this study.

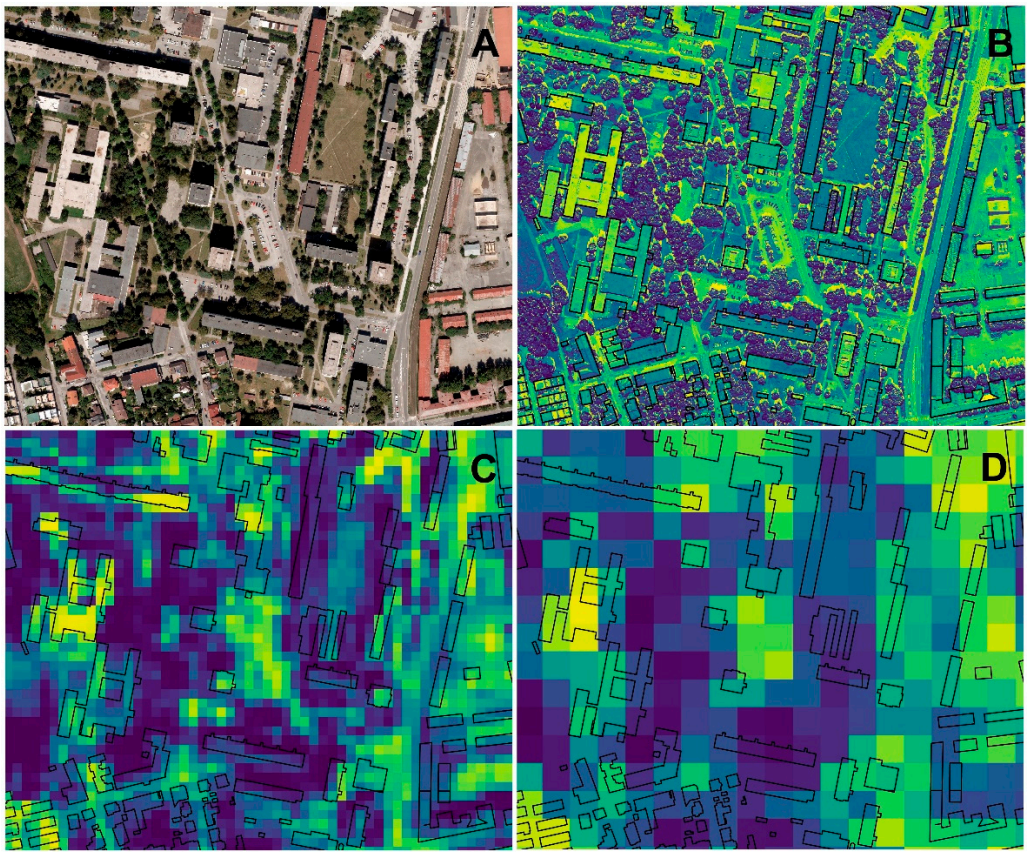

Figure 9. The zoom-in comparison of (**A**): orthophotograph, (**B**): VIS RGB albedo, (**C**): S2 albedo, (**D**): L8 albedo.

4. Discussion

The proposed methodology to derive VIS albedo from RGB orthophotographs requires a high-resolution DSM and information on RGB orthophotograph acquisition time to calculate incident solar irradiance. The brightness component in the HSB color model is used to approximate the light reflected to an RGB sensor. All procedural steps can be

completed using a standard GIS software. The calibration of the VIS albedo values can be completed using appropriate in situ (field-based) or published reference VIS albedo values. The use of widely available aerial RGB orthophotographs along with a high-resolution DSM often derived from increasingly available 3D city models enables the calculation of VIS albedo at the same high spatial resolution. This is an important advantage for further environmental and solar energy urban studies.

It should be noted that VIS albedo can be also directly calculated using accurate RGB bands spectral information of the camera and recorded reflectance in these bands via a weighted mean of single RGB reflectances. However, this information is not always available, especially for simple UAS cameras or orthophotographs of unknown origin.

Despite the fact that the VIS band radiation covers only a small segment of the electromagnetic spectrum, it is a very important segment of the electromagnetic spectrum representing about 46% of available solar energy. For example, visible band radiation has numerous biological effects including a plant photosynthesis (also known as photosynthetically active radiation, PAR) and human sleeping process. Moreover, it can be used to estimate broadband albedo using appropriate conversion formulae (e.g., [8]).

The suggested approach can be also used to estimate direct or diffuse source of VIS albedo, as the r.sun solar radiation model calculates these components of solar irradiance separately. The shadows cast by tall buildings can be used to estimate the diffuse source of VIS albedo. The diffuse component of solar irradiance also helped to partially eliminate the effect of shadows on orthophotographs so the VIS albedo was estimated also for shadowed areas (see Figure 1 vs. Figure 6). The share of diffuse solar irradiance component is strongly affected by Linke's turbidity coefficient. In our case we used only an approximate value typical for this urban area.

The means of derived VIS RGB albedo values based on land cover classes (Figure 6, Table 2) are comparable to VIS albedo derived from Landsat 8 OLI using the Liang [8] methodology, Sentinel 2A using the Li et al. [19] methodology as well as reference values published by Brest [24]. The calibration procedure can be further improved using in situ field measurements of albedo especially for homogeneous land cover classes such as asphalt roads, concrete pavements or roofs. The estimation accuracy is influenced by the accuracy of input and calibration data. Probably the most problematic are urban greenery land cover classes such as parks and gardens with mixed patterns of trees and grass. These also exhibit strong seasonal changes in albedo.

It should be noted that the methodology is also applicable to oblique RGB photographs. If the position of an RGB sensor is known, the angular information of reflected light can be calculated. Oblique aerial photographs are increasingly popular especially in urban areas in mapping vertical surfaces such as facades [27]. The incident solar irradiance on vertical urban surfaces can be calculated using a 3D solar radiation model such as v.sun [28]. The methodology can be also used for infrared aerial orthophotographs and consumer-grade UAV cameras with NIR sensors. The resulting data can be used to create a false-color infrared image that can be treated similarly as in the RGB case.

5. Conclusions

Visible band albedo can be used in many environmental and solar radiation applications. While the satellite-derived albedos can be used in many large-scale applications including the study of UHI effects, there is a growing need for extremely high-resolution data. We proposed a simple methodology based on the usage of widely available aerial orthophotographs to derive VIS albedo that can be effectively used in many urban studies. The solution is based on the ratio of reflected and incident solar irradiance for a given moment. The reflected irradiance is derived using the HSB color model where the brightness component approximates the amount of reflected irradiance. Solar irradiance is calculated using the r.sun solar radiation model. The method was applied to the central area of Košice and compared to the satellite-based albedo and published reference VIS albedo data. The results confirmed the applicability of the proposed methodology with acceptable accuracy.

The methodology is also applicable to oblique photographs increasingly popular in the mapping of vertical surfaces in urban areas.

Author Contributions: Conceptualization, J.H.; methodology, J.H. and K.O.; validation, K.O.; formal analysis, J.H. and K.O.; writing—original draft preparation, J.H. and K.O.; visualization, J.H.; funding acquisition, J.H. All authors have read and agreed to the published version of the manuscript.

Funding: This research was funded by the Slovak Research and Development Agency (APVV) under the contracts No. APVV-18-0044 and by the Scientific Grant Agency of the Ministry of Education, Science, Research and Sport of the Slovak Republic and the Slovak Academy of Sciences (VEGA) under the contract No. 1/0300/19.

Institutional Review Board Statement: Not applicable.

Informed Consent Statement: Not applicable.

Data Availability Statement: The data presented in this study are available on request from the corresponding author. The data are not publicly available due to privacy reasons.

Acknowledgments: We would like to thank Jozef Šupinský and Ján Šašak for providing a technical support in preparing a digital surface model used in this study.

Conflicts of Interest: The author declares no conflict of interest. The funders had no role in the design of the study; in the collection, analyses, or interpretation of data; in the writing of the manuscript, or in the decision to publish the results.

References

1. Bonafoni, S.; Baldinelli, G.; Rotili, A.; Verducci, P. Albedo and surface temperature relation in urban areas: Analysis with different sensors. In *2017 Joint Urban Remote Sensing Event (JURSE)*; IEEE: Dubai, United Arab Emirates, 2017; pp. 1–4. [CrossRef]
2. Roesch, A.; Wild, M.; Pinker, R.; Ohmura, A. Comparison of spectral surface albedos and their impact on the general circulation model simulated surface climate. *J. Geophys. Res.* **2002**, *107*, 4221. [CrossRef]
3. Xue, Y.; Sellers, P.; Kinter, J., III; Shukla, J. A simplified biosphere model for global climate studies. *J. Clim.* **1991**, *4*, 345–364. [CrossRef]
4. Sellers, P.; Randall, D.A.; Collatz, G.J.; Berry, J.A.; Field, C.B.; Dazlich, D.A.; Zhang, C.; Collelo, G.D.; Bounoua, L. A revised land surface parameterization (SiB2) for atmospheric GCMs: Part I. Model formulation. *J. Clim.* **1996**, *9*, 676–705. [CrossRef]
5. Jacobowitz, H.; Tighe, R.J. The earth radiation budget derived from the Nimbus-7 ERB experiment. *J. Geophys. Res.* **1984**, *89*, 4997–5010. [CrossRef]
6. Smith, G.L.; Green, R.N.; Raschke, E.; Avis, L.M.; Suttles, J.T.; Wielicki, B.A.; Davies, R. Inversion methods for satellite studies of the earth's radiation budget: Development of algorithms for the ERBE mission. *Rev. Geophys.* **1986**, *24*, 407–421. [CrossRef]
7. Kandel, R.; Viollier, M.; Raberanto, P.; Duvel, J.P.; Pakhomov, L.A.; Golovko, V.A.; Trishchenko, A.P.; Mueller, J.; Rashke, E.; Stuhlmann, R. The ScaRaB earth radiation budget dataset. *Bull. Am. Meteorol. Soc.* **1998**, *79*, 765–783. [CrossRef]
8. Liang, S. Narrowband to broadband conversions of land surface albedo I: Algorithms. *Remote Sens. Environ.* **2001**, *76*, 213–238. [CrossRef]
9. Brest, C.L.; Goward, S.N. Deriving surface albedo measurements from narrow band satellite data. *Int. J. Remote Sens.* **1987**, *8*, 351–367. [CrossRef]
10. Qu, Y.; Liang, S.; Liu, Q.; He, T.; Liu, S.; Li, X. Mapping Surface Broadband Albedo from Satellite Observations: A Review of Literatures on Algorithms and Products. *Remote Sens.* **2015**, *7*, 990–1020. [CrossRef]
11. Bonafoni, S.; Sekertekin, A. Albedo Retrieval from Sentinel-2 by New Narrow-to-Broadband Conversion Coefficients. *IEEE Geosci. Remote Sens. Lett.* **2020**, *17*, 1618–1622. [CrossRef]
12. Schlosser, A.D.; Szabó, G.; Bertalan, L.; Varga, Z.; Enyedi, P.; Szabó, S. Building Extraction Using Orthophotos and Dense Point Cloud Derived from Visual Band Aerial Imagery Based on Machine Learning and Segmentation. *Remote Sens.* **2020**, *12*, 2397. [CrossRef]
13. Colomina, I.; Molina, P. Unmanned aerial systems for photogrammetry and remote sensing: A review. *ISPRS J. Photogramm. Remote Sens.* **2014**, *92*, 79–97. [CrossRef]
14. Hofierka, J.; Gallay, M.; Onačillová, K.; Hofierka, J., Jr. Physically-based land surface temperature modeling in urban areas using a 3-D city model and multispectral satellite data. *Urban Clim.* **2020**, *31*, 100566. [CrossRef]
15. Hofierka, J.; Bogľarský, J.; Kolečanský, Š.; Enderova, A. Modeling Diurnal Changes in Land Surface Temperature in Urban Areas under Cloudy Conditions. *ISPRS Int. J. Geo-Inf.* **2020**, *9*, 534. [CrossRef]
16. Hofierka, J.; Gallay, M.; Kaňuk, J.; Šupinský, J.; Šašak, J. High-resolution urban greenery mapping for micro-climate modelling based on 3-D city models. *Int. Arch. Photogramm. Remote Sens. Spat. Inf. Sci.* **2017**, *XLII-4/W7*, 7–12. [CrossRef]
17. GRASS GIS. Available online: http://grass.osgeo.org/ (accessed on 4 August 2021).

18. Neteler, M.; Mitasova, H. *Open Source GIS: A GRASS GIS Approach*, 3rd ed.; The International Series in Engineering and Computer Science; Springer: New York, NY, USA, 2008.
19. Li, Z.; Erb, A.; Sun, Q.; Liu, Y.; Shuai, Y.; Wang, Z.; Boucher, P.; Schaaf, C. Preliminary assessment of 20-m surface albedo retrievals from sentinel-2A surface reflectance and MODIS/VIIRS surface anisotropy measures. *Remote Sens. Environ.* **2018**, *217*, 352–365. [CrossRef]
20. Horn, B.K.P. Understanding Image Intensities. *Artif. Intell.* **1977**, *8*, 201–231. [CrossRef]
21. Šúri, M.; Hofierka, J. A New GIS-based Solar Radiation Model and Its Application to Photovoltaic Assessments. *Trans. GIS* **2004**, *8*, 175–190. [CrossRef]
22. Muneer, T.; Guymard, C.; Kambezidis, H. *Solar Radiation and Daylight Models*, 2nd ed.; Elsevier Butterworth-Heinemann: Oxford, UK, 2004.
23. Fairchild, M.D. *Color Appearance Models*, 3rd ed.; Wiley-IS&T Series in Imaging Science and Technology: New York, NY, USA, 2013.
24. Brest, C.L. Seasonal Albedo of an Urban/Rural Landscape from Satellite Observations. *J. Clim. Appl. Meteorol.* **1987**, *26*, 1169–1187. [CrossRef]
25. Kittler, R.; Mikler, J. *Základy Využívania Slnečného Žiarenia*; VEDA: Bratislava, Slovakia, 1986.
26. Spitters, C.J.T.; Toussaint, H.A.J.M.; Goudriaan, J. Separating the diffuse and direct component of global radiation and its implications for modeling canopy photosynthesis Part I. Components of incoming radiation. *Agric. For. Meteorol.* **1986**, *38*, 217–229. [CrossRef]
27. Aicardi, I.; Chiabrando, F.; Grasso, N.; Lingua, A.M.; Noardo, F.; Spanò, A. UAV photogrammetry with oblique images: First analysis on data acquisition and processing. *Int. Arch. Photogramm. Remote Sens. Spat. Inf. Sci.* **2016**, *41*, 835–842. [CrossRef]
28. Hofierka, J.; Zlocha, M. A New 3-D Solar Radiation Model for 3-D City Models. *Trans. GIS* **2012**, *16*, 681–690. [CrossRef]